

IMPACT EXPERIMENTS ON DIFFERENTLY REINFORCED CONCRETE PLATES

Franz Bracklow¹, Marcus Hering², Birgit Beckmann², Manfred Curbach³

¹ Dipl.-Ing. (FH), Institute of Concrete Structures, Dresden, Germany (franz.bracklow@tu-dresden.de)

² Dr.-Ing., Institute of Concrete Structures, Dresden, Germany

³ Univ.-Prof. Dr.-Ing. Dr.-Ing. E.h., Institute of Concrete Structures, Dresden, Germany

ABSTRACT

To investigate the influence of different bending and shear reinforcement configurations of 1.50 x 1.50 x 0.20 m³ reinforced concrete (RC) plates under impact loading, five experiments were carried out at the drop tower facility of the Otto Mohr Laboratory of the Technische Universität Dresden, using the accelerated mode. Therefore, three different arrangements of the flexural reinforcement and two specimens with various stirrup configurations were investigated by using an equal impact velocity. Finally, the relation between global behaviour and local damage of the RC specimens was analysed. It also became clear that the perforation behaviour as well as the fracture body shape at the inside of the tested specimen were influenced by changing the rebar spacing and adding additional stirrups.

INTRODUCTION

The behaviour of reinforced concrete under impact loading has always been of great importance, for instance to protect the critical infrastructure. Due to this fact, impact experiments on concrete specimen with different sizes and reinforcement properties have been conducted worldwide since the middle of the 20th century. One of the famous test series are the Meppen experiments from 1982 with ten large-scale tests on 6.50 m plates, in total. For these tests, bending reinforcement ratios between 0.8% and 1.4% as well as shear reinforcements between 0.1% and 0.5% were used. The deformable projectiles reached velocities up to 260 m/s, Jonas et al. (1982). In year 1986, Eibl and Kreuser (1986) conducted hard impact experiments using 2.7 m RC plates and velocities up to 20 m/s. The reinforcement ratios were between 0.5% and 1.9% for bending reinforcement as well as between 0.5% and 1.0% for stirrup reinforcement. An addition of both test series was performed by Sugano et al. (1993) in 1993 with experiments using soft and hard impact. In total, 83 small, intermediate and large-scaled specimens were tested by using a wide velocity range. In the course of time, impact experiments were conducted on further specified test specimens. For example, Orbovic et al. (2015), among others, tested prestressed and punching-reinforced plates under hard impact in 2013.

All experiments described have in common that the results form the basis for the development of numerical formulae for estimating the material behaviour as well as engineering models and numerical simulations. To advance this developments, own investigations on RC plates under hard impact have been realised at Institute of Concrete Structures since 2012 (see e.g., Beckmann et al. (2012), Just et al. (2016), Hering et al. (2017), Bracklow et al. (2021)). Subsequently described experiments represent a selected part of the previous mentioned investigations.

EXPERIMENTAL PROGRAMME

To investigate the influence of different bending and shear reinforcement configurations, in total five impact experiments on RC plates with a size of 1.50 x 1.50 x 0.20 m³ were conducted. Starting from a base

configuration, the bending reinforcement was varied in one series and the shear force reinforcement in another (Figure 1). All plates were manufactured with ready-mixed concrete, grade C35/45, and differ only in the used reinforcement properties.

Bending Reinforcement		Base Configuration	Shear Reinforcement	
Ø8 mm - 5 cm no stirrups	Ø8 mm - 20 cm no stirrups	Ø8 mm - 10 cm no stirrups	Ø8 mm - 10 cm 32 pc. Ø10 mm	Ø8 mm - 10 cm 60 pc. Ø10 mm

Figure 1. Test matrix

The base configuration consisted of B 500 S reinforcement bars with a diameter of 8 mm which were used with a spacing of 10 cm within two layers (top & bottom). This led to a reinforcement content of 0.5%. In context of the test series "Bending Reinforcement", two more specimens with identical reinforcement diameters but different grid sizes of 5 cm and 20 cm were analysed. The corresponding reinforcement contents were 1.01% and 0.25%. For the "Shear Reinforcement" series, two more plates with the bending reinforcement properties of the base configuration (ø8 mm – 10 cm) were scheduled. In addition, 32 and 60 stirrups respectively were added to these plates between the bending reinforcement layers. This results in stirrup reinforcement contents of 0.11% and 0.22%. In the middle of the plates, Z-shaped and on the edges C-shaped stirrups were used. The concrete cover was 2.5 cm for all specimens.

DROP TOWER EXPERIMENTS

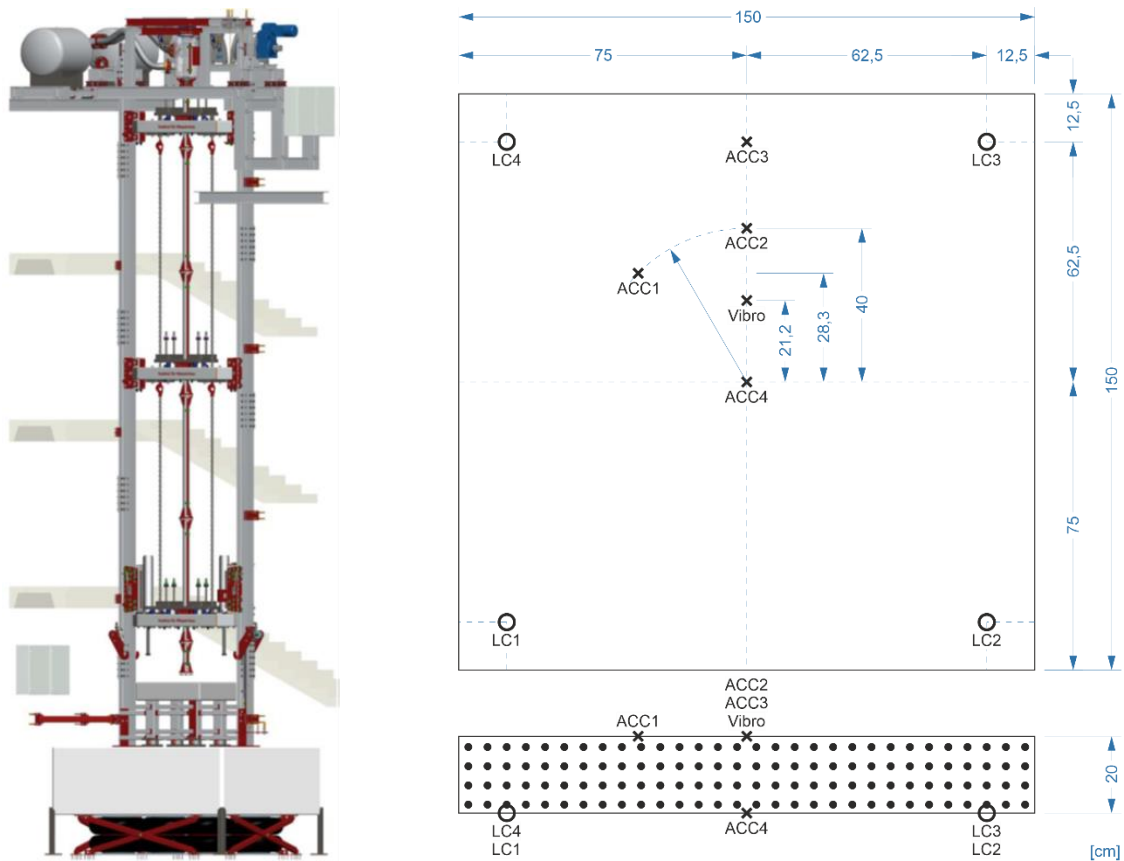


Figure 2. Accelerated configuration of the drop tower facility (left) Graphic: Tino Kühn; Measurement plan (right) Graphic: Franz Bracklow

For conducting the subsequently described impact experiments, the drop tower facility of the Otto-Mohr-Laboratory which is located at the Technische Universität Dresden was used. The accelerated configuration of the facility was applied, wherein projectiles get accelerated to the required impact velocity by using compressed air (see Figure 2). For this purpose, a volume of two vessels with 500 litre each, applicable with a pressure of up to 16 bar was available for using an impactor with a maximal mass of 100 kg. More information is given by Just et al. (2016).

For the experiments presented in this contribution, a flat shaped and 380 mm long steel impactor with a diameter of 10 cm was used. This led to an impact mass of 21.66 kg. From the investigations of the influence of different slap thicknesses on the impact resistance of RC, conducted by Hering et al. (2019), the behaviour of 20 cm thick plates with base configuration (ø8 mm – 10 cm) under impact with different impact velocities was already known. Five velocity levels were considered. The damage varied between the initial formation of a fracture body at 25.2 m/s (1 bar facility pressure) until the complete perforation of the impactor occurred at 61.4 m/s (8 bar). It was visible, that the highest possible load of the specimens occurred at a velocity below the perforation limit. Due to this fact, this loading level was defined as significant for the present investigation of the different reinforcement configurations, corresponding to a facility pressure of 6 bar and a target velocity of about 54 m/s.

The realisation of impact experiments on the structural level leads to huge effort due to the specimen size and the short-term loading. In order to gain the most possible knowledge from this test, a measurement concept was developed to record the support forces, displacements and accelerations of the plates as well as further important parameters for example impact velocity.

The support forces were measured at all corners with four load cells (LC). By using a laser Doppler-vibrometer (Vibro) on the plates' top side, the local displacement could be recorded close to the specimen centre and the impact location. In contrast, the measurement of the global displacements of the specimen was carried out on the basis of a photogrammetric evaluation (GOM) of high-speed camera records of the plates' front side. Further the accelerations on the plate surface were measured by means of four piezoelectric sensors (ACC) to gain inferences of the impact induced damage. The sensor locations were chosen in the way mainly oscillations of the first eigenmode were recorded, see Hering (2020) and Hering et al. (2020). The exact position of the described measurement technique is given at the measurement plan in Figure 2. Further information of the measurement technique used as well as their evaluation and filtering of the raw data is given in Hering et al. (2017) and Bracklow et al. (2021).

EXPERIMENTAL RESULTS

Table 1 summarises the test parameter as well as the observed failure modes of the tested plates. For almost all experiments, the aimed impact velocity of approximately 54 m/s was realised. Only the experiments on plates 227 and 232 showed some deviations due to occurred problems with the acceleration unit.

Table 1: Test parameters and occurred failure mode of all impact experiments.

plate	size [m]	reinforcement		velocity [m/s]	failure mode (h_{imp} $v_{mp,res}$)
		bending	shear		
122	1.50 x 1.50 x 0.20	ø8 mm – 10 cm	-	53.90	global, rebound (30 mm < 0 m/s)
210			32 pc. ø10 mm	53.33	global/local, penetration (78 mm 0 m/s)
216			60 pc. ø10 mm	53.33	global, rebound (38 mm < 0 m/s)
227		ø8 mm – 5 cm	-	48.41	global, rebound (15 mm < 0 m/s)
232		ø8 mm – 20 cm	-	51.25	local, perforation (200 mm 8.28 m/s)

With rebound, penetration and perforation of the impactor, impact experiments can be categorised into three failure modes in general. Rebound is characterised by an acceleration of the impactor in opposite direction after the impact as a consequence of a global structural behaviour. This leads to a negative residual

velocity of the impactor ($v_{imp,res} < 0$), its determination facility related was not possible. To classify the tests despite this lack of information, the penetration depth (h_{imp}) of the impactor is given with the assumption, an increase of the depth leads to a decrease of the residual velocity. If the impactor is decelerated completely by intrusion into the specimen, it is called penetration ($v_{imp,res} = 0$) which corresponds to a hybrid of global and local structural behaviour. For this case, the impact velocity used is close as possible to the theoretical perforation velocity. If the impactor leaves the specimen after the impact on the rear side with a positive residual velocity ($v_{imp,res} > 0$), perforation occurred as a consequence of a local structural behaviour. This parameter could be recorded with the existing measurement technology.

Due to the occurred rebound in connection with the smallest penetration depths, the highest resistance to the applied impact load can be attested to the plates with only bending reinforcement with spacing of 5 cm and 10 cm (no. 122 & 227). A more exact evaluation is not meaningful due to the differences of the impact velocities used of more than 5 m/s. With a 38 mm penetrating rebound as well as a complete penetration of the impactor, the plates with 60 and 32 stirrups (plates no 210, 216) showed less resistance. The worst behaviour was exhibited by the plate no. 232 with 20 cm rebar spacing and without stirrups because a perforation with a considerable residual velocity occurred despite the low impact velocity.

Sensor Signals

Figure 3 und Figure 4 show the curves of the support forces and displacements measured according the measurement plan in Figure 2 as a function of a unique time scale, starting at the moment of the impact at 0 ms. The graphs of the bearing reactions result from the sum of the measured values of all four load cells.

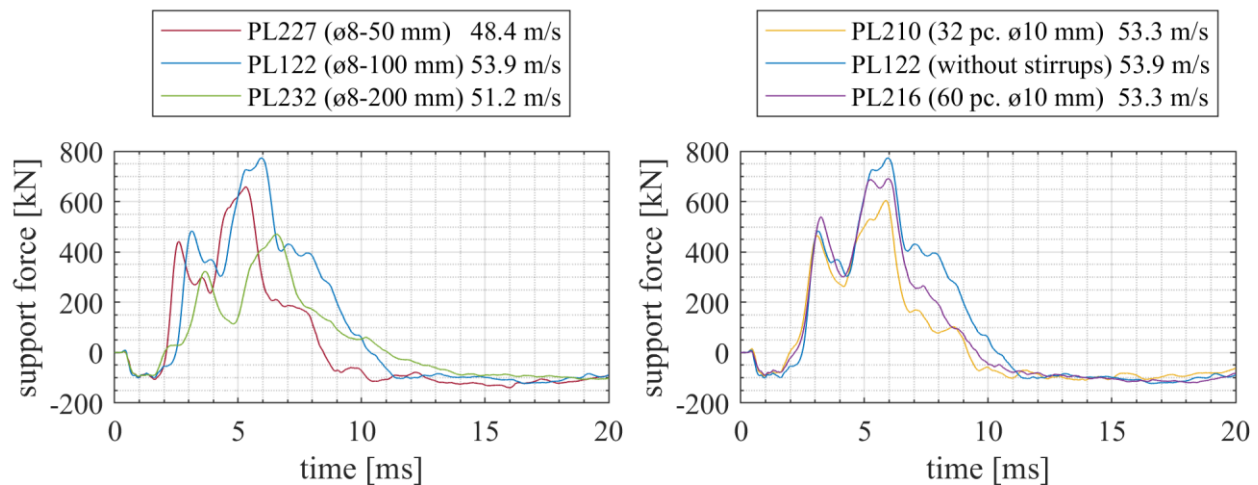


Figure 3. Support forces of test series bending reinforcement (left) and shear reinforcement (right)

To avoid the lifting of the specimen, all plates were fixed with a force of approximately 25 kN on the load cells. This results in the negative course of approximately 100 kN at the beginning of the measurements followed by a further increase until the maximum value was reached. With 471 kN the smallest forces of all tested samples were measured at plate 232. As already mentioned, the complete perforation of the impactor occurred within this experiment as a consequence of a local failure. A sufficient global behaviour for distributing the impact force could not be achieved and only low support forces were measured. In contrast, plates 227 and 122 showed a substantial higher local stiffness which led to the large support forces of 659 kN and 774 kN. Contrary to the expectations, the configuration with the reinforcement mesh of 10 cm reached the highest bearing reactions. Probably, the significantly low impact velocity on the plate with a spacing of 5 cm is the reason for this unexpected result.

Comparing the specimens with stirrup reinforcements, it is visible that both shear reinforcement ratios used results in decreasing support reactions, comparing the reference plate 122 without stirrups. With a value of 774 kN, this specimen achieved a higher load than the 32 stirrups plate 210 (606 kN) as well as the 60 stirrups plate 216 with 692 kN. Similar to the experiment on plate 232, it seems that the stirrup reinforced plates showed a reduced local stiffness. An explanation for this behaviour can be found with the localisation of the occurred damage which will be further explained in the later sections of the fracture body analysis.

Figure 4 gives the displacement-time curves measured by using a vibrometer or photogrammetry. For all plates, the local deformations measured closely to the impact show considerably higher values than the displacements recorded globally at the front side of the plate, from whose curves the eigenmode-caused bulging of the plate edge is additionally visible. Despite the distance as well as the different curve characteristics of both measurements, the displacements measured by vibrometer and by using photogrammetry reached the maximum values almost simultaneously.

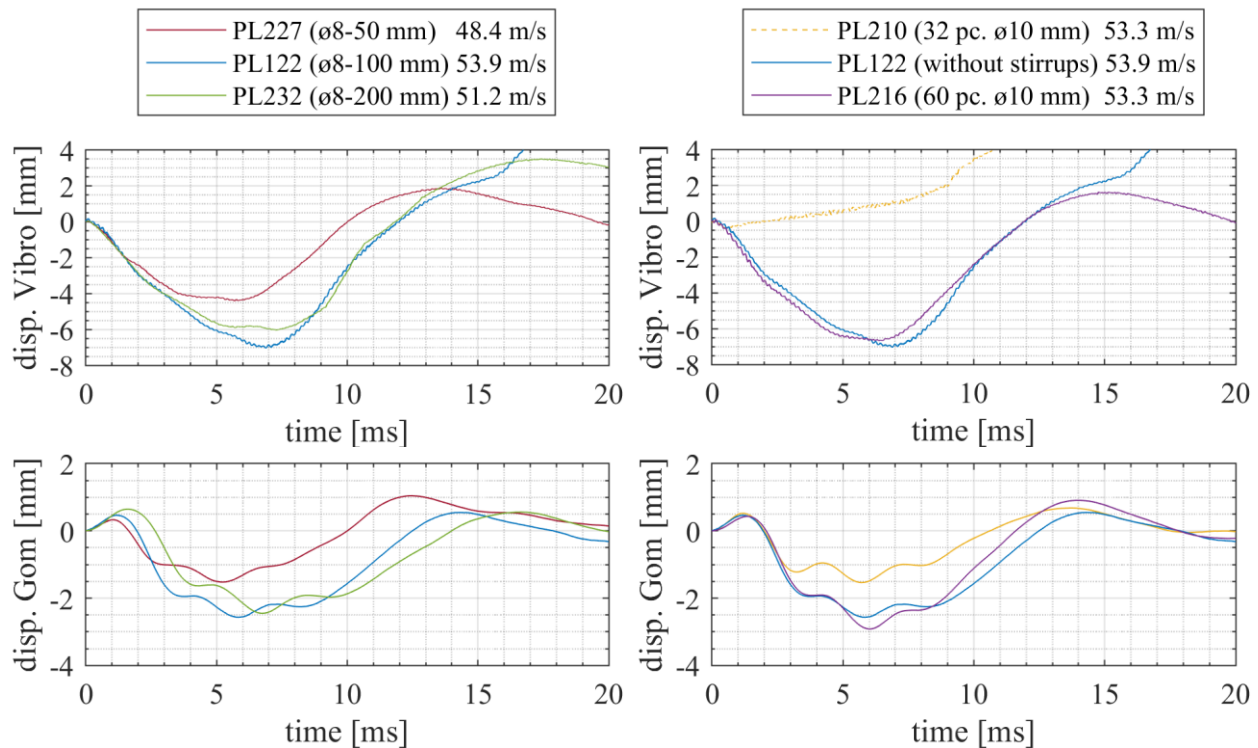


Figure 4. Displacements measured by vibrometer (centre of plate, top) and photogrammetry (plate's front side, bottom) of test series bending reinforcement (left) and shear reinforcement (right)

Due to the global structural behaviour, the largest displacements with 7.1 mm and 2.6 mm (Vibro/GOM) were measured at the reference plate. Despite the higher plate stiffness, it was expected that a smaller grid size of 5 cm led to similar values as a consequence of the lower support forces. But smaller deflections were measured of 4.1 mm and 1.5 mm, which is probably due to the low impact velocity. As a consequence of the occurred perforation, besides the small support forces additionally displacements of 6.1 mm and 2.5 mm were measured on plate 232. Due to the local failure, these values are lower than the reference plate 122 but higher than originally expected.

At plate 210 of the shear reinforcement series, a mismeasurement of the vibrometer took place as a result of spalling. Hence, the movement of concrete fracture was measured which is not corresponding to the plate deflection. The displacement of 1.5 mm evaluated by the photogrammetry reflects the increasing

local failure. In contrast, plates 122 and 216 (6.7 mm and 2.9 mm) with identical global behaviour according to Table 1, exhibit similar support responses and more or less identical deflections too.

Analytical Damage Evaluation

To compare the occurred damage, both global and local damage parameters according to Hering (2020) and Hering et al. (2020) were determined. For evaluating the global damage degrees (Θ_{global}), the differences between the plate stiffness before and after the impact experiments were determined. For this purpose, the oscillatory responses of the specimens after a manually stimulation were measured with the acceleration sensors (ACC) depicted at Figure 3. Subsequently, the eigenfrequencies were derived from these signals by using a fast Fourier transform for evaluating the specimen stiffnesses. The local damages were divided into top ($\Theta_{\text{local,Spalling}}$) and bottom side ($\Theta_{\text{local,Scabbing}}$) damage degree. For determining these parameters, the weight of the scabbing and spalling failure masses, respectively, after the impact were related to the total mass of the plate before the experiment.

Figure 5 represents respective damages for all specimens dependent from the impact velocity. For the plates with different bending reinforcement spacing, plate 227 shows the lowest total damage with 33%, followed by slab 232 with 41%. The highest value was achieved by the reference specimen 122 with 46%. This led to the assumption that the global damage increases with larger rebar distances except changes in the failure mode (perforation at plate no. 232). However, a relation between the impact velocity and the occurred damage is visible, which means higher impact intensity causes higher global failure. Regarding the local behaviour it can be recognized that a reduction of the rebar spacing led to a decreasing scabbing with 40%, 21% and 12% as well as increasing spalling with 0‰, 0‰ and 1.2‰.

The plates 210 and 216 with additional shear reinforcements have the same global damage with 47%. Despite the lower velocity, these values are slightly higher than for the reference specimen 122 with 46%. Under consideration of the local behaviour, this tendency can be obtained too. With 26% and 15%, the scabbing values are close to the 21% of the reference plate but 1.4‰ and 0.5‰ spalling represents a significant increase in damage related to 0‰ of plate 122.

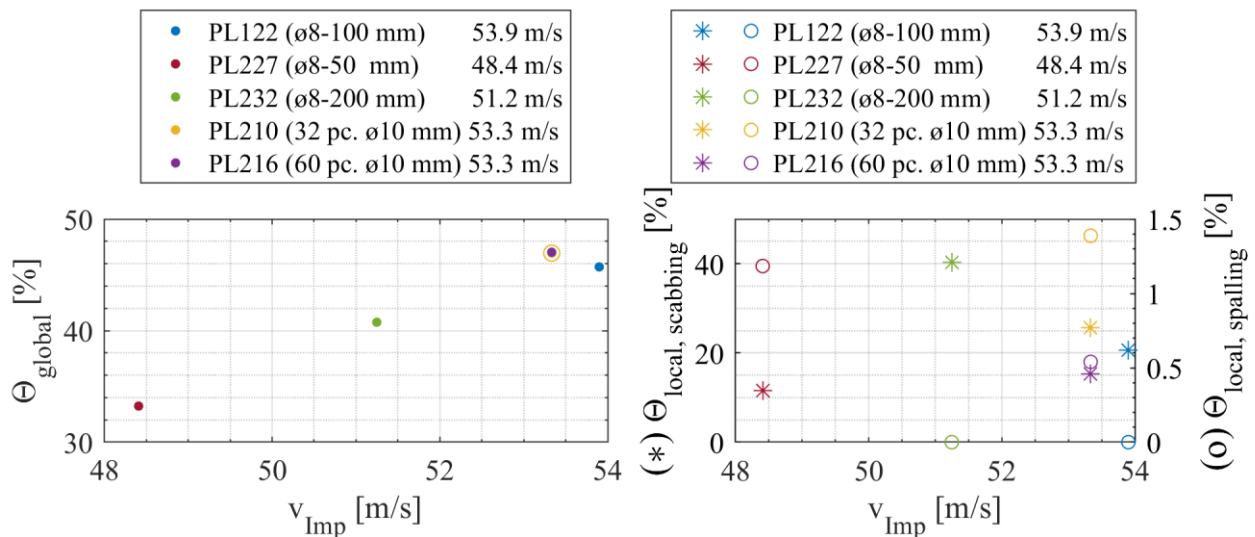


Figure 5. Analytical damage evaluation, global damage (left), local damage (right)

Fracture Body Analysis

After the test execution, all tested specimens were sawed in the middle to investigate the fracture body and analyse possible differences due to the different bending and shear reinforcement configurations. Figure 6

shows the cross sections of all specimens. For both series, reference plate 122 represents the comparative cross section.

Besides the main fracture body in the middle of the plate, the cross section of plate 227 also shows further lateral cracks moving from the top side to the lower reinforcement and causes a secondary fracture body. Except this increasing crack formation, the interior of both fracture bodies is mostly undamaged. Only some areas of the concrete cover on the top and rear side were detached due to the impact. In addition to the enlarged detachment of the concrete cover on the bottom side on plate 122, also an increased fragmentation and removing of the punching cone is visible. Simultaneously, the formation of a second fracture body is also recognisable, but in contrast to plate 227 only on the left side of the punching cone. As a consequence of the perforation of plate 232, the punching cone was almost completely crushed out of the specimen. Furthermore, lateral cracks from a second fracture body, as seen on the previous plates, are not visible.

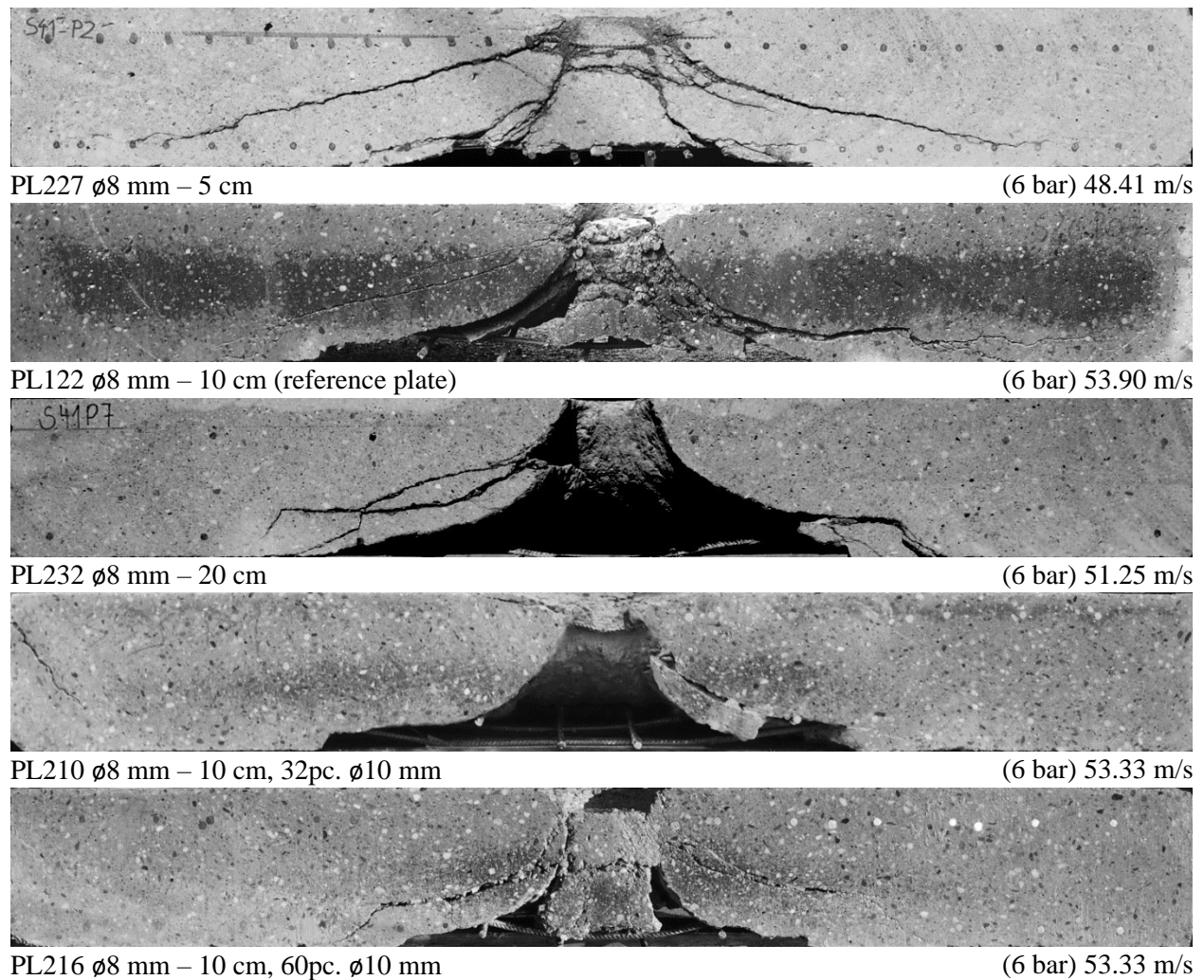


Figure 6. Cross sections of all tested specimen

As mentioned before, a fragmented and partly detached primary as well as a half-sided secondary fracture body occurred at reference plate 122. Compared to the specimens without additional shear reinforcement, the compact shape of the punching cones of plates 210 and 216 is obvious. The fracture body is only partially removed on the plate with 60 stirrups, but almost completely crushed out on the plate with 32 stirrups. Further cracks besides the punching cones are not visible.

Besides the visual evaluation, further approaches for an analytical description of the fracture body are given for comparing the different reinforcement configurations. The approximation of the fracture body boundaries by using a cubic function, described by Hering (2020) and Hering et al. (2020), is the basis for these considerations. By analysing the resulting polynomials, it is possible to derive characteristic values for the resulting fracture pattern. In Figure 7, this procedure is given for the reference plate 122 according to Bracklow et al. (2021). The polynomials of the fracture body boundaries were plotted in blue within the picture of the cross section. By determining and labelling the tangents in the middle of the plate height, the punching angles (α) could be defined for both, the primary and secondary fracture body with the slopes. Furthermore, the analysis of the inflection points of the polynomials was used to evaluate the localisation of the occurred fracture patterns. For this purpose, the distances of the inflection points (Δ_{IP}) were compared with each other.

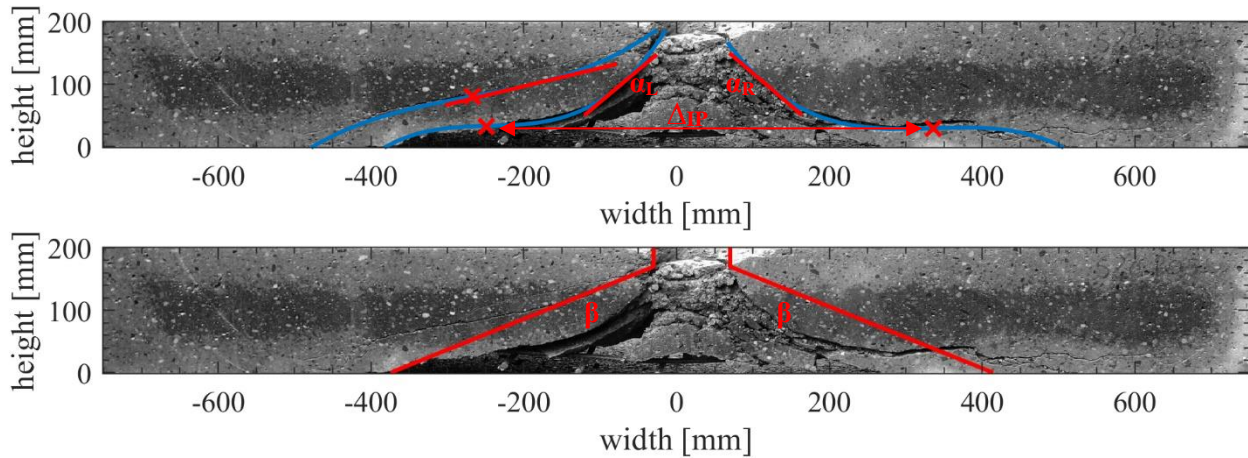


Figure 7. Fracture body description of plate 122, analysing α and Δ_{IP} (above), β (below)

$$\beta = \tan^{-1} \left(\frac{h_{slab} - h_{Impact}}{(\phi_{Scabbing} - \phi_{Impactor}) \cdot 0.5} \right) \quad (1)$$

All plates depicted at Figure 6 were evaluated with respect to these described parameters, and the results for both the primary and secondary fracture bodies are given in Table 2. Another commonly used procedure to determine the punching angle is given by Equation (1), considering the scabbing diameter ($\phi_{Scabbing}$) and the penetration depth (h_{Impact}) of the impactor (see Figure 7). For comparing this approach with the procedure described according to the above scheme, the calculated punching angle (β) is also given within the table.

Table 2: Parameters of graphical damage evaluation.

plate	punching cone			primary fracture body			secondary fracture body		
	h_{Impact} [mm]	$\phi_{Scabbing}$ [cm]	β [°]	α_L α_R [°]	α_m [°]	Δ_{IP} [cm]	α_L α_R [°]	α_m [°]	Δ_{IP} [cm]
122	30	79	26	46 46	46	58	16 -	16	-
210	(78)*	68	34	51 43	47	51	- -	-	-
216	38	72	28	41 21	31	47	- -	-	-
227	15	60	37	48 65	56.5	41	13 25	19	77
232	(200)*	82	29	26 41	33.5	56	- -	-	-

*an impact depth 0 mm was used for evaluating β according to equation (1) due to the global/local respectively local failure mode

Comparing the different punching angles β and α , it is recognisable that both values show the same tendency despite small deviations. The calculated β -values consistently result in flat inclined angles as a consequence of the truncated cone-shaped fracture body described by Equation (1). The determination by using the tangent incline of the real punching body shape seems to provide more realistic results in this respect. Another advantage is the possibility of analysing further fracture bodies, for example of the already mentioned secondary cone, within the same conditions. Due to these reasons, the further analysis will be realised by using the α -values in combination with the inflection point distance (Δ_{IP}) to consider the different characteristics of the lower damage range too. For a better comparison, the approximated fracture bodies of the both test series analysed in Table 2 are additionally shown in Figure 8.

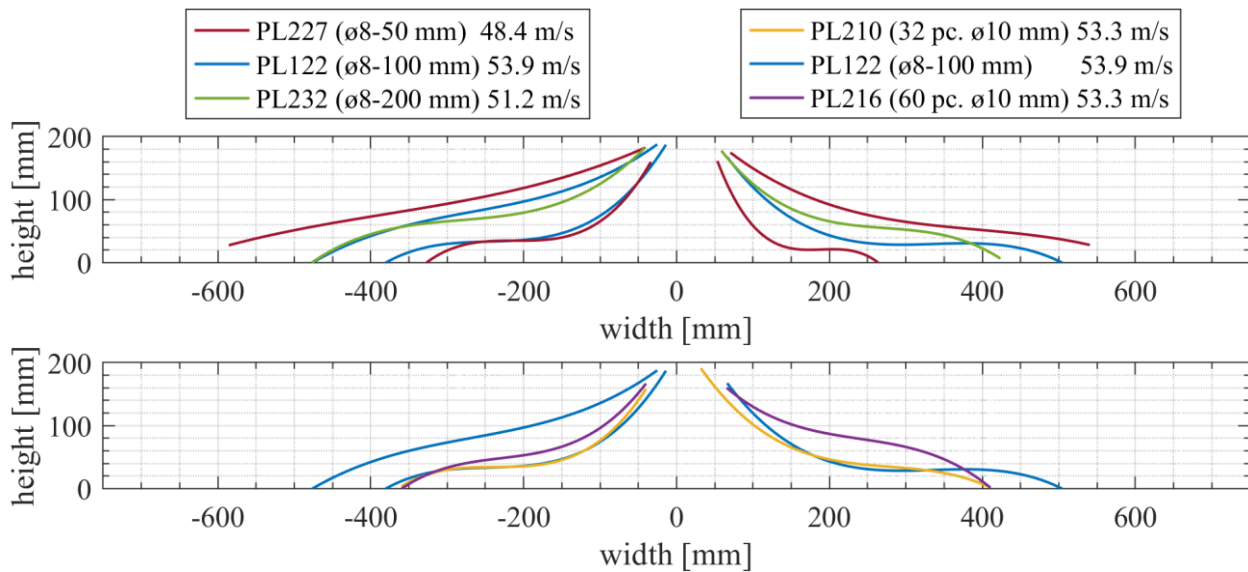


Figure 8. Graphical fracture body evaluation

In the context of the flexural RC plates, the punching angles decrease from 56.5° to 46° and 33.5° by decreasing the reinforcement distance. Simultaneously, the tendency for a second fracture body decreases. With values of 16° and 19° , the resulting angles are equal, but flatter than the primary fracture body in the middle. The distance of the inflection points increases from 41 cm on plate 227 to 58 cm and 56 cm on plate 122 and 232. As can be seen in Figure 8, the lower fracture region of plate 232 also shifts towards the centre of the plate to the level of the secondary fracture bodies of plates 227 and 122. It can be summarised that a reinforcement spacing of 5 cm led to a very localised fracture body as a consequence of a membrane effect of the small reinforcement grid. As a result, the areas beside the punching cone were also activated, leading to the forming of further cracks of a secondary fracture body. This overall behaviour decreases at plate 122 and especially at plate 232 with increasing reinforcement distance of 10 cm and 20 cm.

In the case of the stirrup reinforced plates 210 and 216, similar punching angles of 47° and 31° but lower inflexion point distances of 51 cm and 47 cm were measured comparing to the reference plate. The increasing stirrup reinforcement ratio led to a similarly localised damage as obtained on plate 227 but no secondary fracture body occurred due to the used stirrups.

CONCLUSIONS AND OUTLOOK

In the frame of two test series, in total five concrete plates with different bending and shear reinforcement configurations were tested under impact loading. For this purpose, a velocity closely below the perforation limit of the reference plate was chosen. A correlation between the occurred structural behaviour and the

measured support forces and displacements was described and the global and local damage was evaluated. Further, an analysis of the fracture body inside the specimen was performed.

Small reinforcement spacing led to an improved global behaviour of the plate due to the membrane effect of the reinforcement layer and caused the formation of multiple fracture bodies. In contrast, the tendency of perforation failure increased with larger grid sizes of the reinforcement due to a reduction in local resistance. This behaviour was also observed in a weak form for plates with stirrups. In this case, the reason is seen in the localised shape of the fracture body. The presented experiments are part of preliminary work for the strengthening of plates under impact loading in the frame of research training group GRK 2250 “Mineral-bonded composites for enhanced structural impact safety”.

ACKNOWLEDGEMENT

The presented investigations were funded by the German Federal Ministry for Economic Affairs and Climate Action (BMWK, projects no. 1501541) on basis of a decision by the German Bundestag as well as by the German Research Foundation (DFG, project no. 287321140) in the frame of Research Training Group GRK 2250, Doctoral Project A5/II. Further thanks belong to the employees of the Otto-Mohr-Laboratory for supporting the experimental investigations as well as Silke Scheerer for reviewing the manuscript.

REFERENCES

- Bracklow, F., Babiker, A., Hering, M., Kühn, T., Curbach, M., Häußler-Combe, U. (2021). *Bauteilverhalten unter stoßartiger Beanspruchung durch aufprallende Behälter (Flugzeugtanks); Phase 1C: Experimentelle und numerische Untersuchungen zu Maßstabeffekten, Versagensmechanismen und Bauteilschädigung*. Final report, Institute of Concrete Structures, Technische Universität Dresden.
- Beckmann, B., Hummeltenberg, A., Weber, T., Curbach, M. (2012). “Strain Behaviour of Concrete Slabs under Impact Load”. *Structural Engineering International* 22 (4), 562–568.
- Eibl, J., Kreuser, K. (1986). *Versuche zum Verhalten unterschiedlicher Stahlsorten in stoßbeanspruchten Platten*. Ernst & Sohn, Berlin.
- Hering, M. (2020). *Untersuchung von mineralisch gebundenen Verstärkungsschichten für Stahlbetonplatten gegen Impaktbeanspruchungen*. Diss., Technische Universität Dresden.
- Hering, M., Bracklow, F., Kühn, T., Curbach, M. (2019). “Impact experiments with reinforced concrete plates of different thicknesses”. *Structural Concrete* 21 (2), 587–598.
- Hering, M., Bracklow, F., Scheerer, S., Curbach, M. (2020). “Reinforced Concrete Plates under Impact Load – Damage Quantification”. *Materials* 13 (20), 4554.
- Hering, M., Kühn, T., Curbach, M. (2017). *Bauteilverhalten unter stoßartiger Beanspruchung durch aufprallende Behälter (Flugzeugtanks); Phase 1B: Quantifizierung der Schädigungen des Betongefüges, Teilprojekt: Fallturmversuche*. Final report, Institute of Concrete Structures, Technische Universität Dresden.
- Jonas, W., Rüdiger, E., Gries, M., Riech, H., Rützel, H. (1982). *Kinetische Grenztragfähigkeit von Stahlbetonplatten 1982. RS 165 – IV. Ultimate kinetic bearing capacity of reinforced concrete slabs*. Final report, Hochtief AG Abt. Kerntechnischer Ingenieurbau.
- Just, M., Curbach, M., Kühn, T., Hering, M. (2016). *Bauteilverhalten unter stoßartiger Beanspruchung durch aufprallende Behälter (Flugzeugtanks); Phase 1A: Maßstabeffekte bei stoßartiger Beanspruchung*. Final report, Institute of Concrete Structures, Technische Universität Dresden.
- Orbovic, N., Sagals, G., Blahoianu, A. (2015). “Influence of transverse reinforcement on perforation resistance of reinforced concrete slabs under hard missile impact”. *Nuclear Engineering and Design* 295, 716–729.
- Sugano, T., Tsubota, H., Kasai, Y., Koshika, N., Ohnuma, H., von Riesenmann, W.A., Bickel, D.C., Parks, M.B. (1993). “Local Damage to Reinforced Concrete Structures Caused by Impact of Aircraft Engine Missiles Part 1. Test Program, Method and Results”. *Nuclear Engineering and Design* 140 (3), 387–405.